Unexpected CNN-to-CC Ligand Rearrangement in Pincer-Ruthenium Pre-catalysts Leads to a Base-Free Catalyst for Ester Hydrogenation

Linh Le, Jiachen Liu, Tianyi He, Jack C. Malek, Tia N. Cervarich, John C. Buttner, John Pham, Jason M. Keith,* and Anthony R. Chianese*

Department of Chemistry, Colgate University, 13 Oak Drive, Hamilton, NY 13346.

ABSTRACT: We report the conversion of a series of CNN-pincer-ruthenium complexes Ru(CNN)HCl(CO) to a CC-chelated form $Ru(CC)(PR_3)_2H(CO)$ on reaction with sodium *tert*-butoxide and monodentate phosphines. When the phosphine is triphenylphosphine, *cis*-phosphine complexes form at room temperature, which convert to the *trans* isomer at elevated temperatures. When the phosphine is tricyclohexylphosphine, only the *trans*-phosphine isomer is observed. The CC-chelated complexes are active catalysts for the hydrogenation of esters, without the need for added base. The ligand structure-activity relationship in the series of CC-chelated complexes mirrors that in the precursor CNN-Ru complexes, potentially indicating a common catalytic mechanism. Density functional theory calculations establish a plausible mechanism for the CNN-to-CC rearrangement and demonstrate that this rearrangement is potentially reversible under the conditions of ester hydrogenation catalysis.

INTRODUCTION

The catalytic hydrogenation and dehydrogenation of polar substrates have advanced significantly in the past decade, since the reports of Milstein and co-workers describing a PNN-pincer-ruthenium complex that is active under mild conditions for the hydrogenation of esters[1] and the reverse reaction, dehydrogenation of primary alcohols to give esters.[2] In this work, it was demonstrated that a CH_2 linker on the pincer ligand can be reversibly deprotonated. This acid/base reactivity of the ligand was proposed to be involved in metal-ligand cooperative activation of dihydrogen and transfer to polar substrates, analogous to the historically significant catalytic systems of Shvo[3] and Noyori[4] for ketone and imine hydrogenation.

Since Milstein's 2006 disclosure, many transition-metal catalysts for ester hydrogenation have been reported, including eight we are aware of that give at least 10,000 turnovers at full substrate conversion.[5] These highly active catalysts employ ruthenium or osmium, and feature ligands designed with the metal-ligand cooperative mechanism in mind. Although the availability of detailed experimental mechanistic information is limited,[5c, 6] computation has offered additional insight into questions that are not easily probed experimentally.[5a, 5c, 6b, 6d, 6f, 7] Recently, the long-accepted involvement of reversible ligand deprotonation as an integral part of the catalytic cycle has been called into question, both for the Noyori ketone hydrogenation system[7k, 8] and for ester hydrogenation catalysts featuring N-H functionality.[6g, 7k] Although many examples exist where synthetic elimination of the N-H functionality by replacement with N-Me, N-Bn, or O, is highly detrimental to catalysis,[5d, 5f, 5h, 6b, 6h, 9] some systems are similarly active[6g, 7k] or more active[10] when N-H is substituted with N-Me. Ester hydrogenation catalysts have also been reported that feature no obvious acidic sites on the ligand.[6c, 7h, 11] To facilitate the development of improved catalysts, it is clearly of continued importance to probe the relationship between catalyst structure and activity in ester hydrogenation and related hydrogenations of polar bonds, and to work to understand the potentially complicated and varied catalytic mechanisms.

Several groups have reported catalysts for ester hydrogenation or the reverse reaction based on pincer N-heterocyclic carbene (NHC) ligands, as shown in Chart 1.[5d, 12] Each catalyst has the possibility of reversible ligand deprotonation, either at an N-H group or CH_2 linker. For their CNN-Ru catalysts, Song and coworkers observed stoichiometric deprotonation at the CH_2 linker arm connecting the NHC and pyridine rings.[12c] Computations indicated that deprotonation at the alternate linker arm connecting the pyridine and NEt_2 groups was less favorable by 9 kcal/mol.

We have reported a series of CNN-pincer ruthenium catalysts for ester hydrogenation, which differs from those of Song and Sánchez in that the pyridine and NHC rings are directly linked, so that the only available site for ligand deprotonation is the CH_2 linker between the pyridine and NR_2 groups.[13] A detailed study of the effect of ligand structure on catalyst activity showed that activity increased with increasing steric bulk on the NHC substituent.[14] A striking effect of the amine substituent was also observed, as NEt_2 or N^iPr_2 groups gave high activity while an NMe_2 group led to greatly diminished activity.

Chart 1. Pincer-NHC catalysts for ester hydrogenation

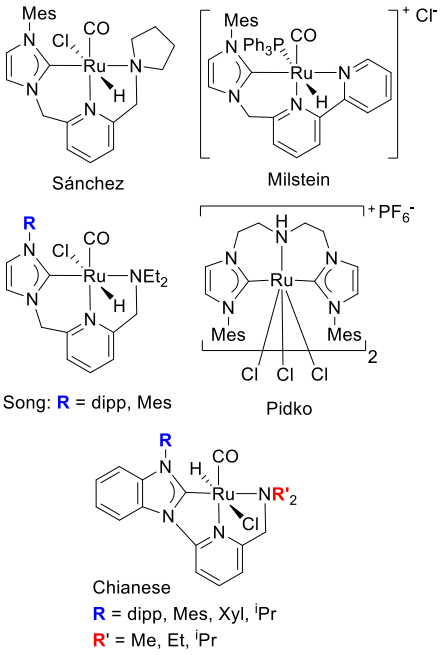

In an effort to understand the catalytic mechanism, we began studying the stoichiometric reactivity of the pre-catalysts in the presence of the strong base, NaO^{t}Bu, required for catalyst activation. In addition to the anticipated deprotonation of the CH_2 linker arm, we also observed an unexpected rearrangement of the complex, where the CNN-pincer ligand converts to a CC-chelating form through C-H activation of the pyridine ring. In this paper, we report the isolation of a series of these rearranged ruthenium complexes and their application as catalysts for ester hydrogenation. We find that the CC-chelated catalysts are effective without the need for a basic additive. Importantly, the structure-activity relationship mirrors that of the precursor CNN-Ru pre-catalysts, potentially indicating a common catalytic mechanism. Through computation, we present an energetically plausible mechanism for the rearrangement and establish that the CNN and CC forms of the catalyst are thermodynamically similar, indicating that either form is thermally accessible under our catalytic conditions.

RESULTS AND DISCUSSION

Formation of Dearomatized CNN-Pincer Ligand with NaO^{t}Bu and Pyridine. Since our CNN-pincer-ruthenium pre-catalysts for ester hydrogenation, shown in Chart 1, require the addition of a strong base for activation, we began by studying the reactivity of these hydridochloride complexes with strong bases such as NaO^{t}Bu and $KN(SiMe_3)_2$. These reactions gave intractable mixtures of ruthenium-containing products for several of our pre-catalyst variants. Song and coworkers noted a similar issue in their work: their 2,6-diisopropylphenyl-substituted variant (see Chart 1) cleanly gave a 5-coordinate species featuring a deprotonated, dearomatized CNN-pincer ligand, while the mesityl-substituted variant gave a mixture of products.[12c] For this complex, a clean deprotonation of the CH_2 linker between the NHC and pyridine rings was observed when PPh_3 was also added to the reaction mixture, allowing formation of a coordinatively saturated species.

When we combined the yellow pincer-ruthenium complex **Ru-dipp-Et** with an excess of NaO^{t}Bu and pyridine in benzene-d_6 at room temperature, we observed rapid formation of a homogenous, red solution, which contained the anticipated dearomatized species **Ru-dipp-Et-pyr**, shown in Scheme 1, as the major species. While we have characterized this complex in solution by ^{1}H NMR, COSY, and NOESY, it decomposed slowly at room temperature, and we were not able to isolate it.

Scheme 1. Reaction with NaO^{t}Bu and pyridine

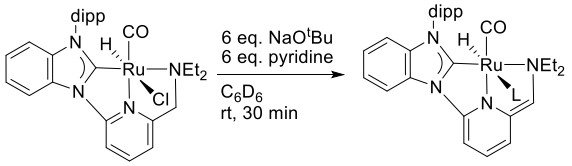

Ru-dipp-Et **Ru-dipp-Et-pyr**, L = pyridine

The ^{1}H NMR spectrum of **Ru-dipp-Et-pyr** shows the lack of symmetry expected for the chiral-at-metal complex shown: four doublet signals are observed for the isopropyl CH_3 groups, two septets are observed representing the isopropyl methine hydrogens, and the two N-ethyl groups are diastereotopic. Signals for Ru-bound pyridine are not observed, which is consistent with fast exchange between free and bound pyridine at room temperature. The Ru-bound hydride is observed at –13.56 ppm. A NOE signal is observed between the hydride and one isopropyl CH_3 group, consistent with the coordination geometry shown in Scheme 1. The upfield shifts of the resonances on the pyridine ring are consistent with dearomatization.[2, 12c]

Interestingly, cross-peaks indicative of chemical exchange were observed by NOESY for resonances representing the diastereotopic N-ethyl groups of **Ru-dipp-Et-pyr**. This observation is consistent with dechelation of the NEt_2 group, inversion about nitrogen, and recoordination to exchange the environments of the two ethyl groups.

CNN-to-CC Rearrangement with NaO^{t}Bu and PPh_3. When we combined the pincer-ruthenium complexes **Ru-Mes-Et** and **Ru-dipp-Et** with an excess of NaO^{t}Bu and PPh_3 in toluene at room temperature, we initially observed complex mixtures, each of which converged to one product overnight. We identified these products as the CC-chelated complexes shown in Scheme 2, where the pyridine and amine nitrogen donors have dissociated, and a pyridine C-H bond has been activated. C-H cyclometallation of pyridine rings is quite common, and has been observed before in closely related systems. Liang and Song observed a similar CC-chelating binding mode in pyridine-NHC complexes of ruthenium and iron.[15] Milstein and coworkers observed a CC-chelating binding mode when attempting complexation of their NHC-bipyridine ligand (see Chart 1) with $Ru(PPh_3)_3HCl(CO)$.[12b] The same group also observed rearrangement of a phosphine-bipyridine PNN-pincer ligand to a PNC-binding form on ruthenium.[16]

Scheme 2. Reaction with NaO^{t}Bu and PPh_3

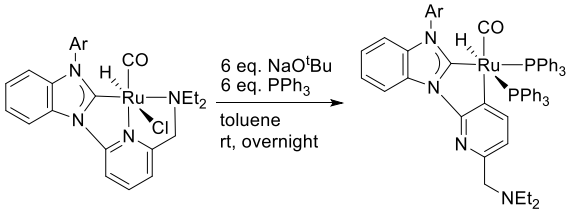

Ru-Mes-Et, Ar = Mes
Ru-dipp-Et, Ar = dipp

***cis*-Ru-Mes-Et-PPh$_3$**, 72%
***cis*-Ru-dipp-Et-PPh$_3$**, 79%

The solid-state structure of ***cis*-Ru-dipp-Et-PPh$_3$** was determined by X-ray crystallography. Figure 1 shows the molecular structure. The geometry is nearly octahedral, distorted by a small 77.5° bite angle for the bidentate ligand and a large 103.7° angle between the PPh_3 ligands. The arrangement of ligands around the metal center is consistent with a lack of isomerization other than the CNN-to-CC rearrangement: the newly added phosphine ligands occupy the sites vacated by the displaced chloride ligand and NEt_2 group of the reactant.

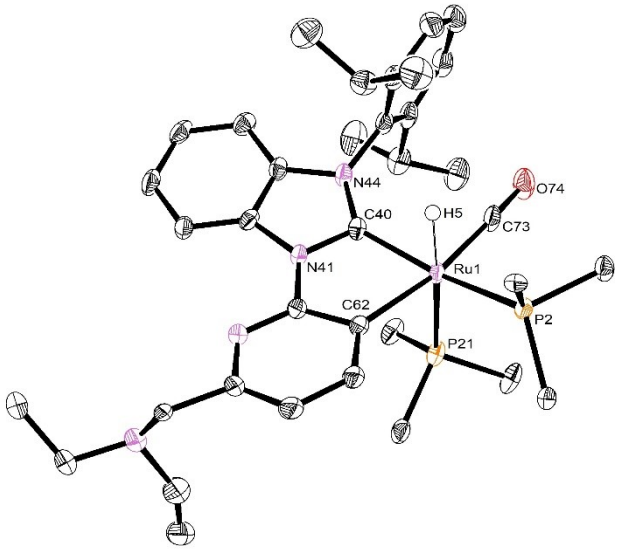

Figure 1. ORTEP diagram of ***cis*-Ru-dipp-Et-PPh$_3$**, showing 50% probability ellipsoids. Phenyl groups and hydrogen atoms other than the ruthenium-hydride are omitted for clarity.

NMR spectroscopy indicates that the solution structures of ***cis*-Ru-Mes-Et-PPh$_3$** and ***cis*-Ru-dipp-Et-PPh$_3$** are consistent with the crystal structure of ***cis*-Ru-dipp-Et-PPh$_3$**. Two ^{31}P resonances are observed for each complex, with small P–P coupling constants of 21.6 and 21.8 Hz, respectively. Each ruthenium hydride appears as a doublet of doublets. The coupling constants between the ruthenium hydride and phosphorus are consistent with one phosphorus *trans* to H and one *cis* to H: 34.4 and 77.4 Hz for ***cis*-Ru-Mes-Et-PPh$_3$**, and 32.3 and 76.1 Hz for ***cis*-Ru-dipp-Et-PPh$_3$**. In the ^{13}C NMR spectrum, each of the CO and carbene resonances appears as a doublet of doublets due to splitting by phosphorus. The CO carbons show two small P–C coupling constants: 13.2 and 6.7 Hz for ***cis*-Ru-Mes-Et-PPh$_3$**, and 10.6 and 7.1 Hz for ***cis*-Ru-dipp-Et-PPh$_3$**, indicating that both phosphine ligands are *cis* to CO. The carbene carbons each show one small and one large P–C constant: 80.4 and 6.0 Hz for ***cis*-Ru-Mes-Et-PPh$_3$**, and 80.4 and 6.7 Hz for ***cis*-Ru-dipp-Et-PPh$_3$**, indicating that one phosphine ligand is *trans* to the NHC.

***Cis-Trans* Isomerization in PPh$_3$ Complexes.** When ***cis*-Ru-Mes-Et-PPh$_3$** is heated at 80° C overnight, an isomerization reaction occurs (Scheme 3). The product was isolated and identified as ***trans*-Ru-Mes-Et-PPh$_3$**, where the hydride and a phosphine ligand have exchanged sites with no other rearrangement at the metal center. The crystal structure was determined; an ORTEP diagram is shown in Figure 2. The coordination geometry is again that of a distorted octahedron. The P–Ru–P angle is 145.6°, as the PPh_3 ligands are bent away from the NHC moiety and toward the hydride, likely to minimize a steric clash between the phenyl groups and the mesityl group.

Scheme 3. Cis-trans isomerization

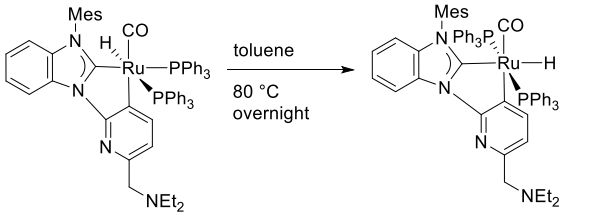

***cis*-Ru-Mes-Et-PPh$_3$** ***trans*-Ru-Mes-Et-PPh$_3$**, 59%

The NMR spectrum of ***trans*-Ru-Mes-Et-PPh$_3$** in solution is consistent with its solid-state structure. Two equivalent phosphorus nuclei are observed. The ruthenium hydride signal appears as a triplet, with a 28.2 Hz coupling constant to phosphorus. The carbonyl and carbene carbons each appear in the ^{13}C NMR spectrum as triplets, with P–C coupling constants of 10.1 and 5.7 Hz, respectively.

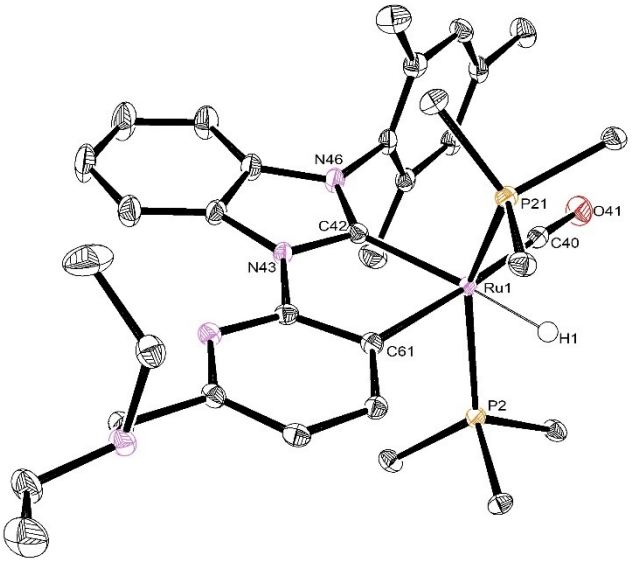

Figure 2. ORTEP diagram of ***trans*-Ru-dipp-Et-PPh$_3$**, showing 50% probability ellipsoids. Phenyl groups and hydrogen atoms other than the ruthenium-hydride are omitted for clarity.

When ***cis*-Ru-dipp-Et-PPh$_3$** is heated at 80° C overnight, an analogous *cis-trans* isomerization occurs. In this instance, an equilibrium is established, with an approximately 1:4 ratio of the *cis* isomer to the *trans* isomer. The ratio of isomers did not change upon further heating, but some decomposition began to occur. Since the *trans* complex was not formed cleanly, we did not attempt to isolate it.

CNN-to-CC Rearrangement with NaO^{t}Bu and PCy$_3$. We observed the same ligand rearrangement reaction when our CNN-pincer ruthenium complexes were combined with NaO^{t}Bu in the presence of tricyclohexylphosphine. Because these products were observed to be highly active catalysts for ester hydrogenation (*vide infra*), we prepared a series of four such CC-chelated complexes, as shown in Scheme 4. In each case, we only observed products where the two PCy_3 ligands were mutually *trans*, presumably because of the larger size of the cyclohexyl group as compared to phenyl.

Scheme 4. Reaction with NaO^{t}Bu and PCy_3

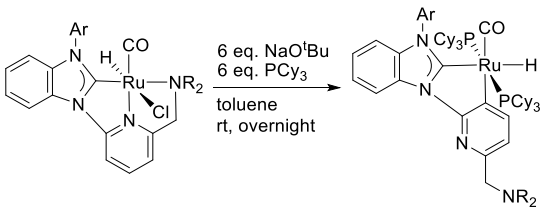

Ru-Mes-Et, Ar = Mes, R = Et
Ru-dipp-Me, Ar = dipp, R = Me
Ru-dipp-Et, Ar = dipp, R = Et
Ru-dipp-^{i}Pr, Ar = dipp, R = ^{i}Pr

Ru-Mes-Et-PCy_3, 43%
Ru-dipp-Me-PCy_3, 25%
Ru-dipp-Et-PCy_3, 35%
Ru-dipp-^{i}Pr-PCy_3, 37%

X-ray crystal structures were determined for three PCy_3 complexes: **Ru-Mes-Et-PCy_3** (Figure 3), **Ru-dipp-Me-PCy_3** (Figure 4), and **Ru-dipp-^{i}Pr-PCy_3** (Figure 5). These three complexes share the same coordination geometry, which is analogous to ***trans*-Ru-Mes-Et-PPh_3**, described above. A noteworthy feature of all three crystal structures of PCy_3 derivatives is a significant distortion away from C_s symmetry, resulting from steric interactions between the bulky PCy_3 ligands and NHC aryl substituents. The lower image in Figure 3, showing the $C_{carbene}$-Ru-$C_{pyridine}$ plane horizontally, demonstrates this distortion. From this perspective, the mesityl group bends upwards while the upper PCy_3 ligand bends away from it. The upper C_{NHC}–Ru-P bond angle is 109.0°, while the analogous lower angle is 100.1°. The distortion results in a non-trivial pyramidalization of an sp^2-hybridized nitrogen in the benzimidazole ring: the N-bound carbon of the mesityl group, C(55), is 0.52 Å away from the mean plane of the NHC ring. The analogous distance (referred to as *x* below) is 0.37 Å for **Ru-dipp-Me-PCy_3** and 0.57 Å for **Ru-dipp-^{i}Pr-PCy_3**.

A search of the Cambridge Structural Database reveals that this distortion is quite unusual.[17] In 9130 published crystal structures where a transition metal is bound to an NHC (based on imidazole or benzimidazole, excluding imidazoline-based structures with a C-C single bond in the five-membered ring), the mean distance *x* is 0.081 Å with a standard deviation of 0.070. Only seven published structures lacking disorder contain a distance *x* greater than 0.50 Å. These structures feature multidentate ligands with an unusually strained chelate ring,[18] a monodentate ligand where the N-substituents are part of a ring fused to the NHC ring,[19] and a monodentate ligand with neopentyl N-substituents, which are very bulky but capable of shifting to one side of the imidazole plane.[20]

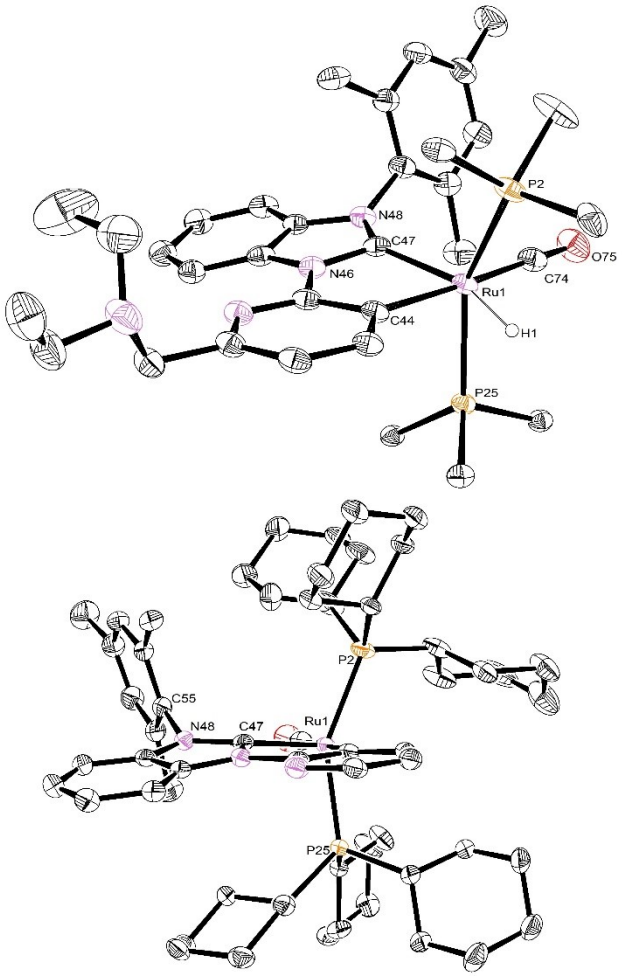

Figure 3. ORTEP diagram of **Ru-Mes-Et-PCy_3**, showing 30% probability ellipsoids. Cyclohexyl groups and hydrogen atoms other than the ruthenium-hydride are omitted for clarity. The lower view shows the distortion away from C_s symmetry.

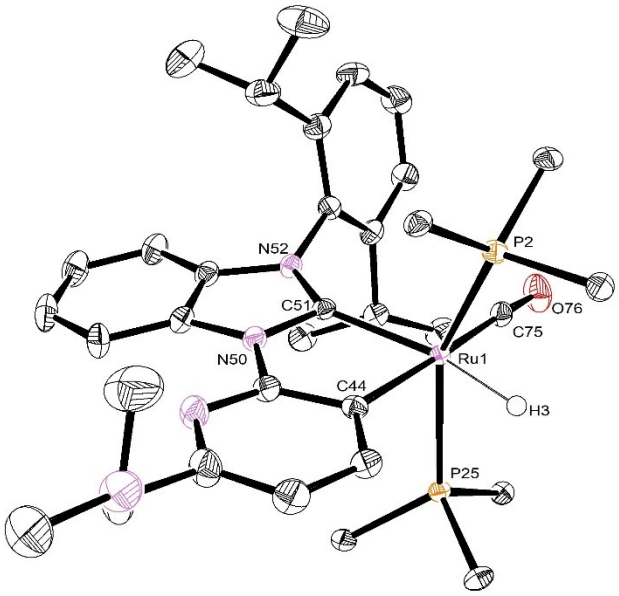

Figure 4. ORTEP diagram of **Ru-dipp-Me-PCy_3**, showing 50% probability ellipsoids. Cyclohexyl groups and hydrogen atoms other than the ruthenium-hydride are omitted for clarity.

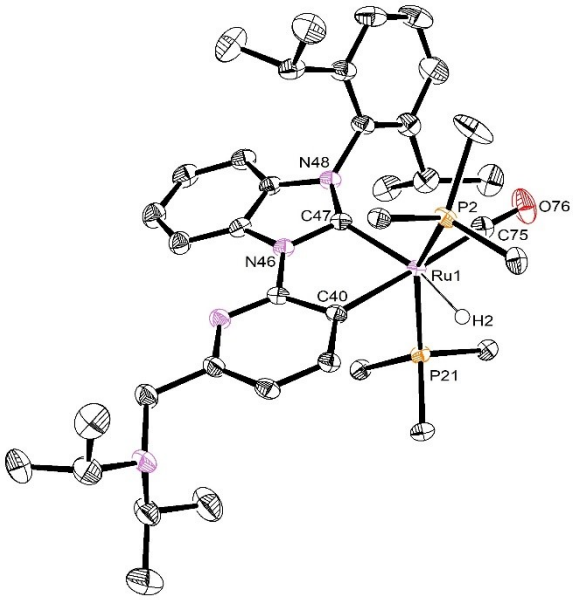

Figure 5. ORTEP diagram of **Ru-dipp-^{i}Pr-PCy$_3$**, showing 50% probability ellipsoids. Cyclohexyl groups and hydrogen atoms other than the ruthenium-hydride are omitted for clarity.

Dynamic Behavior of *Trans*-PCy$_3$ Complexes. The four PCy$_3$ complexes described in the above paragraph exhibited dynamic behavior in solution, as observed by NMR spectroscopy. At room temperature, broad resonances are observed for nuclei that would be chemically equivalent if the complex possessed a time-averaged mirror plane coincident with the CC ligand. To characterize this dynamic behavior, ^{1}H and ^{31}P NMR spectra were collected at 220 K. At this temperature, the NMR spectra are consistent with C_1-symmetry. Two inequivalent ^{31}P resonances are observed for each complex, and each ruthenium hydride appears as a doublet of doublets rather than a triplet. ^{1}H resonances for the ortho and meta substituents on the N-aryl rings, mesityl or 2,6-diisopropylphenyl, de-coalesce, as do those for the two hydrogens on the CH_2-linker. From this data, it is not straightforward to determine whether the three cyclohexyl groups on each phosphine ligand are equivalent, so it is not clear whether rotation about the Ru-P bonds is fast or slow at 220 K.

Although it is conceivable that the low-symmetry complexes observed at low temperature are different from the solid-state structures determined by X-ray crystallography – *cis*-PCy$_3$ species for example – the P-P and H-P coupling constants offer strong evidence against this. For the four complexes, $^{2}J_{PP}$ ranges from 195 to 206 Hz, much larger than is typical for *cis*-phosphine complexes. P-H coupling constants, measurable for **Ru-dipp-Me-PCy$_3$** and **Ru-dipp-Me-PCy$_3$**, range from 26.9 to 35.0 Hz, consistent with the hydrides being *cis* to both phosphorus ligands in each complex. We propose that the structure in solution closely mirrors that observed in the solid state, where the PCy$_3$ ligands are nearly *trans*. In this case, a motion (Scheme 5) where the N-aryl group flips from up to down, while the upper phosphine ligand moves in and the lower phosphine moves out, is consistent with the chemical exchange behavior observed by NMR.

Scheme 5. Dynamic process in PCy$_3$ complexes

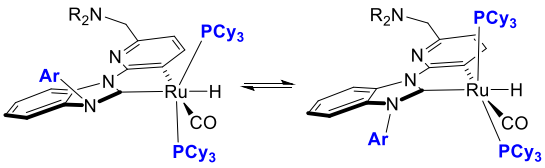

Ester Hydrogenation: Catalyst Comparison. The CNN-Ru precursors to the rearranged, CC-chelated complexes described above form catalysts for ester hydrogenation upon activation with NaO^{t}Bu.[13-14] Our previous ester hydrogenation experiments were conducted at 105 °C, while the CNN-to-CC ligand rearrangements occur at room temperature. Although phosphine ligands were not added to catalytic reactions in our previous work, it is plausible that a similar ligand rearrangement occurs during catalysis, potentially as a pathway for activation or deactivation. To probe for this possibility, we tested the new CC-chelated complexes as catalysts for the hydrogenation of ethyl benzoate.

Table 1. Comparison of CC-Chelated Catalysts[a]

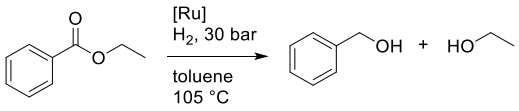

Entry	[Ru]	mol %	% Yield
1	***cis*-Ru-Mes-Et-PPh$_3$**	0.2	>99
2	***cis*-Ru-dipp-Et-PPh$_3$**	0.2	98
3	**Ru-Mes-Et-PCy$_3$**	0.2	>99
4	**Ru-dipp-Me-PCy$_3$**	0.8	29
5	**Ru-dipp-Et-PCy$_3$**	0.1	99
6	**Ru-dipp-^{i}Pr-PCy$_3$**	0.2	98

[a]Each reaction was carried out at a range of catalyst loadings; the lowest loading giving at least 95% yield is reported.

Table 1 shows the results of this catalyst comparison. Most of the newly synthesized complexes are effective catalysts for the hydrogenation of ethyl benzoate under the conditions employed. Although the addition of a strong base was required for the CNN-Ru precursors, these CC-chelated complexes are active without an additive. The highest turnover number of 990 was observed for **Ru-dipp-Et-PCy$_3$**; notably, this was the most effective ligand in our previous work employing the CNN-pincer form of these catalysts, with *in-situ* activation by NaO^{t}Bu.[14]

It is especially noteworthy that **Ru-dipp-Me-PCy$_3$** forms a poor catalyst for this transformation, while a simple change of the NMe$_2$ group to NEt$_2$ or N^{i}Pr$_2$ results in high activity. The same effect was observed in our previous work: pre-catalysts with an NMe$_2$ group were nearly inactive, while those featuring an NEt$_2$ or N^{i}Pr$_2$ group were highly active once activated with NaO^{t}Bu.[14] The observation of the same subtle ligand effect on catalytic activity for both sets of complexes suggests that they may share a common catalytic intermediate (*vide infra*).

Ester Hydrogenation: Substrate Scope. With the identification of **Ru-dipp-Et-PCy$_3$** as the catalyst of choice, we studied its activity for the hydrogenation of a range of ester substrates (Table 2). Full conversion to the alcohol products was obtained for aromatic and aliphatic esters. The lactone

phthalide (Entry 5) was not fully hydrogenated, even at the highest catalyst loading tested.

Table 2. Substrate Scope[a]

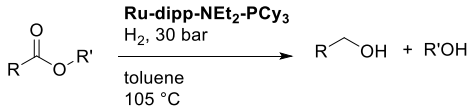

Entry	Substrate	mol %	% Yield
1	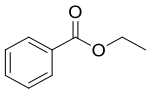	0.1	99
2	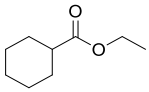	0.2	>99
3	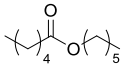	0.2	99
4	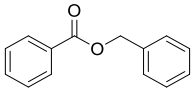	0.8	>99
5	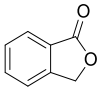	0.8	81
6	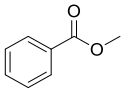	0.05	>99
7	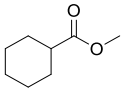	0.1	>99
8	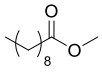	0.4	>99
9[b]	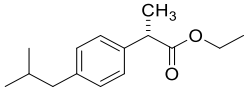	0.8	86, 98% ee

[a]Each reaction was carried out at a range of catalyst loadings; the lowest loading giving at least 95% yield is reported. [b]The reactant (*S*)-ethyl ibuprofen had >99% ee, as determined by GC.

The ability to hydrogenate esters in the absence of an added strong base[6c] may be useful when base has the potential to cause undesired side reactions. For example, alkoxide bases are known to catalyze the racemization of α-chiral esters, which has been exploited in the dynamic kinetic resolution of racemic esters via hydrogenation.[9, 21] On the other hand, if the ester reactant is enantiopure, a loss of optical purity would be detrimental. Kuriyama and coworkers have reported the use of a pre-activated catalyst in the hydrogenation of α-chiral esters with minimal loss of optical purity.[22] Clarke has successfully employed the weaker base K_2CO_3 in Mn-catalyzed ester hydrogenation, which also allows retention of chirality for *α*-chiral esters.[23] We attempted the hydrogenation of (*S*)-ethyl ibuprofen, catalyzed by **Ru-dipp-Et-PCy$_3$** with no basic additive (Entry 9). Although only 86% yield was obtained at the highest catalyst loading attempted, a minimal loss of enantiopurity was observed, from 99% in the reactant to 98% in the product. Further investigations of the applications of base-free ester hydrogenation are in progress.

Mechanistic Analysis of CNN-to-CC Rearrangement by DFT. As noted in the Introduction, all of the most active catalysts for ester hydrogenation have been designed with the metal-ligand cooperative (MLC) mechanism in mind. The same is largely true for the broader class of catalysts for the hydrogenation and dehydrogenation of polar C-O and C-N bonds, notable exceptions being catalysts based on the tripodal "triphos" family of ligands[7h, 11, 24] and the Cp*-Ir-bipyridine system recently reported by Sanford and Goldberg.[6c]

The CC-chelated complex **Ru-dipp-NEt$_2$-PCy$_3$** and its analogs have no potentially basic ligand site in close proximity to the metal, as required for the MLC mechanism. If the ligands retained this binding mode in the catalytic cycle, an MLC mechanism would likely not be operative, a finding which could have broad implications for catalyst design. To probe this possibility, we began by assessing the mechanism of the CNN-to-CC ligand rearrangement using density functional theory.

First, we assessed the relative thermodynamic stability at 298.15 K of four ruthenium complexes that might plausibly form by reaction of **Ru-dipp-Et** with a strong base in the presence of PCy_3 (Chart 2). The species with the lowest free energy is **B**, an 18-electron, five-coordinate, square-planar ruthenium(0) complex formed by formal reductive elimination of HCl from **Ru-dipp-Et** and addition of one PCy_3 ligand. The 4-coordinate, 16-electron square-planar complex **A**, formed by removal of PCy_3, is higher in free energy by 8.5 kcal/mol. The isomeric ruthenium(II) hydride complexes **A-dearom** and **B-dearom**, resulting from deprotonation of the CH_2 linker instead of the metal center, were calculated to be higher in free energy by 10.5 and 6.1 kcal/mol, respectively. Note that **B-dearom** is structurally analogous to the spectroscopically observed complex **Ru-dipp-Et-pyr** (*vide supra*), except that the monodentate ligand L is PCy_3 rather than pyridine.

Chart 2. Thermodynamic comparison of possible products of HCl elimination from Ru-dipp-Et (L = PCy$_3$)

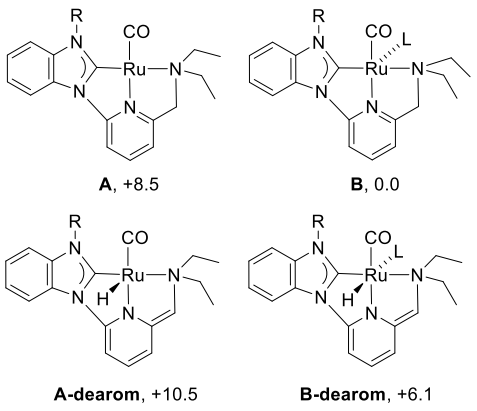

We then identified an energetically plausible pathway for the conversion of **B** into the observed product **Ru-dipp-Et-PCy$_3$**, as detailed in Figure 6. First **B** converts to **C** by dechelation of the NEt_2 arm. Decoordination of the pyridine nitrogen and rotation around the $N_{benzimidazole}$-$C_{pyridine}$ bond via **CD-TS** gives **D**, a C-H σ-complex. C-H oxidative addition then proceeds through **DE-TS** to give **E**, a 16-electron, five-coordinate ruthenium(II) species where the vacant site is trans to the newly formed hydride ligand. An associatively induced isomerization through transition-state **EP-TS** gives **Ru-dipp-Et-PCy$_3$**, where the hydride has moved trans to the NHC and the incoming PCy_3 ligand binds trans to the previously bound PCy_3. At 298.15 K,

the overall rearrangement of **B** to **Ru-dipp-Et-PCy$_3$** is calculated to be thermodynamically favorable by 9.3 kcal/mol.

We have also calculated the relative free energies of the species in Figure 6 at 378.15 K or 105 °C, the operating temperature of the catalytic reactions reported above. At this temperature, the conversion of **Ru-dipp-Et-PCy$_3$** back to **B** is calculated to be thermodynamically uphill by only 5.9 kcal/mol, with a highest barrier of 23.5 kcal/mol through **CD-TS** (see Table S1 for the complete list of energies). Therefore, it is plausible that the CC-chelated pre-catalysts we have synthesized serve as a latent form of a catalytically active CNN-pincer complex under our catalytic conditions. Because of the dramatic effect of the amine alkyl substituents on catalytic activity, we believe catalysis through a CNN-pincer binding mode is probable.

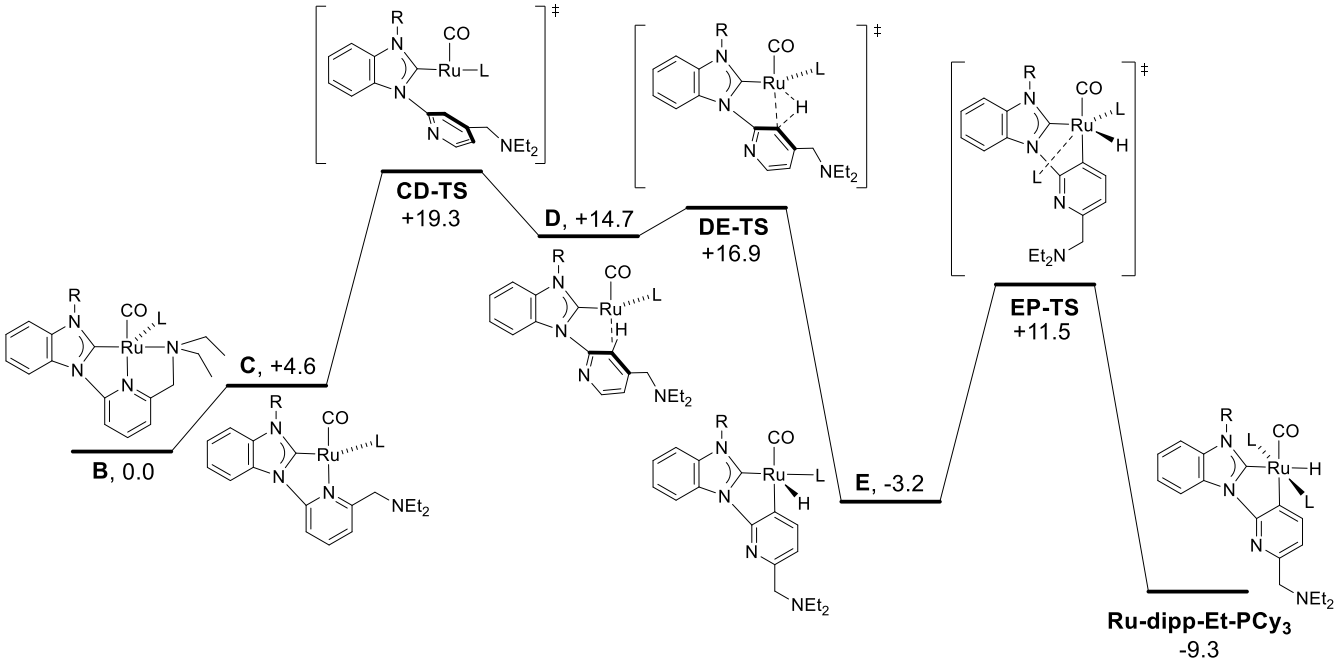

Figure 6. Free energy profile for the conversion of **B** into **Ru-dipp-Et-PCy$_3$** via dechelation of the pincer ligand followed by C-H activation. Solvent-corrected free energies at 298.15 K are given in kcal/mol.

CONCLUSION

In summary, we have demonstrated that a class of CNN-pincer ruthenium pre-catalysts for ester hydrogenation undergoes an unusual rearrangement to a CC-chelated form in the presence of NaO^{t}Bu and phosphine ligands. The CC-chelated complexes are highly active catalysts for ester hydrogenation, without the requirement of exogenous base. Computational analysis showed that reversion to a catalytically active CNN-chelated form is possible under the conditions employed. A detailed experimental and computational investigation of the catalytic reaction mechanism is in progress.

EXPERIMENTAL SECTION

General Methods. Unless stated otherwise, all reactions were carried out either on a Schlenk line under argon or in an argon-filled MBraun Labmaster 130 glovebox. Solvents were purified by sparging with argon and passing through columns of activated alumina, using an MBraun Solvent Purification System. All reagents and materials were commercially available and were used as received, unless otherwise noted. NMR spectra were recorded at room temperature on a Bruker spectrometer (400 MHz for ^{1}H NMR and 100 MHz for ^{13}C NMR) and referenced to the residual solvent resonance (δ in parts per million, J in Hz). Elemental analyses were performed by Robertson Microlit, Madison, NJ. Detailed NMR assignments for the newly reported ruthenium complexes are given in the Supporting Information.

Air-Free Gradient Flash Chromatography. Complexes ***trans*-Ru-Mes-Et-PPh$_3$**, **Ru-Mes-Et-PCy$_3$**, **Ru-dipp-Me-PCy$_3$**, **Ru-dipp-Et-PCy$_3$**, and **Ru-dipp-^{i}Pr-PCy$_3$** did not survive silica gel chromatography in air, but were air-stable in dichloromethane/ethyl acetate solution for at least an hour. These complexes were purified by gradient flash chromatography using a Teledyne Isco Combiflash RF system, taking precautions to exclude air while the compounds were in contact with silica gel. Nitrogen was supplied to the gas intake of the Combiflash system. The prepacked silica-gel cartridge to be used was installed and purged with nitrogen for 30 minutes before loading the samples. The chromatography solvents were sparged with nitrogen for 30 minutes before loading the samples and continually during chromatography. Solvent pumps were primed three times with degassed solvent before introducing solvent to the column. To load the sample, the crude reaction mixture in toluene was filtered through a PTFE disc in the glovebox, transferred to a capped plastic syringe, and removed from the glovebox along with a separate syringe containing 10 mL of degassed dichloromethane. At the start of the chromatographic run, the filtered reaction solution was injected, followed by the dichoromethane chaser. As purified product eluted, the solution was immediately transferred to a round-bottom flask, and the solvent was removed by rotary evaporation. Purified, dried samples were stored in the glovebox.

Ru-dipp-Et-pyr. In the glovebox, **Ru-dipp-Et** (10 mg, 0.017 mmol), pyridine (8 mg, 0.1 mmol), and NaO^{t}Bu (9.5 mg, 0.099 mmol) were combined in 0.5 mL C_6D_6 and stirred at room

temperature for 30 minutes to give a red solution. This solution was transferred to a J-Young NMR tube and NMR spectra were recorded at room temperature. This complex decomposed slowly at room temperature in solution or upon removal of solvent, and was not isolated. ^{1}H NMR (C_6D_6): δ 7.59 (d, $^3J_{HH}$ = 8.1 Hz, 1H, $CH_{benzimid}$); 7.53 (t, $^3J_{HH}$ = 7.8 Hz, 1H, CH_{dipp}); 7.42 (d, $^3J_{HH}$ = 7.8 Hz, 1H, CH_{dipp}); 7.34 (d, $^3J_{HH}$ = 7.8 Hz, 1H, CH_{dipp}); 6.95 (t, $^3J_{HH}$ = 7.8 Hz, 1H, $CH_{benzimid}$); 6.85-6.80 (m overlapped with free pyridine, $CH_{benzimid}$ and $CH_{pyridine}$); 6.46 (d, $^3J_{HH}$ = 7.8 Hz, 1H, $CH_{benzimid}$); 6.10 (d, $^3J_{HH}$ = 9.1 Hz, 1H, CH_{pyr}); 5.82 (d, $^3J_{HH}$ = 6.8 Hz, 1H, $CH_{pyridine}$); 4.41 (s, 1H, CH_{linker}); 3.28 (m, NCH_2CH$_3$); 3.12 (m, NCH_2CH$_3$); 2.76 (sept, $^3J_{HH}$ = 6.8 Hz, 1H, CH_{iPr}); 2.47-2.36 (m, 2H, NCH_2CH$_3$ and CH_{iPr}); 2.14 (m, 1H, NCH_2CH$_3$); 1.61 (d, $^3J_{HH}$ = 7.0 Hz, 3H, $CH_{3\text{-}iPr}$); 1.27 (t, $^3J_{HH}$ = 6.8 Hz, 3H, NCH$_2$CH_3); 1.00 (t, $^3J_{HH}$ = 6.8 Hz, 3H, NCH$_2$CH_3); 0.95 (d, $^3J_{HH}$ = 7.0 Hz, 3H, $CH_{3\text{-}iPr}$); 0.93 (d, $^3J_{HH}$ = 7.0 Hz, 3H, $CH_{3\text{-}iPr}$); 0.77 (d, $^3J_{HH}$ = 7.0 Hz, 3H, $CH_{3\text{-}iPr}$); -13.46 (s, 1H, Ru*H*).

***cis*-Ru-Mes-Et-PPh$_3$**. In the glove box, **Ru-Mes-Et** (75 mg, 0.13 mmol), a stir bar, triphenylphosphine (209 mg, 0.80 mmol), NaO^{t}Bu (77 mg, 0.80 mmol), and benzene (4 mL) were added to a vial and stirred overnight at room temperature. The mixture was filtered through a PTFE disk and layered with 30 mL pentane, which resulted in the slow precipitation of a white solid. The solid was washed with pentane and dried under vacuum. Yield: 96 mg, 72%. ^{1}H NMR (CD_2Cl_2): δ 8.81 (d, $^3J_{HH}$ = 8.0 Hz, 1H, $CH_{benzimid}$); 7.40 (m, 6H, CH_{PPh3}); 7.19 (t, $^3J_{HH}$ = 7.8 Hz, 1H, $CH_{benzimid}$); 7.13 (t, $^3J_{HH}$ = 7.8 Hz, 3H, CH_{PPh3}); 7.06 (t, $^3J_{HH}$ = 7.8 Hz, 3H, CH_{PPh3}); 7.03 (t, $^3J_{HH}$ = 7.8 Hz, 1H, $CH_{benzimid}$); 7.01 (t, $^3J_{HH}$ = 7.8 Hz, 6H, CH_{PPh3}); 6.97 (s, 1H, CH_{Mes}); 6.92 (s, 1H, CH_{Mes}); 6.88 (t, $^3J_{HH}$ = 7.4 Hz, 6H, CH_{PPh3}); 6.69 (m, 6H, CH_{PPh3}); 6.55 (d, $^3J_{HH}$ = 8.1 Hz, 1H, $CH_{benzimid}$); 6.40 (dd, $^3J_{HH}$ = 7.6 Hz, $^4J_{HP}$ = 1.4 Hz, 1H, CH_{pyr}); 6.15 (d, $^3J_{HH}$ = 7.4 Hz, 1H, CH_{pyr}); 3.55 (s, 2H, CH_2NEt$_2$); 2.46 (q, $^3J_{HH}$ = 7.2 Hz, 4H, NCH_2CH$_3$); 2.29 (s, 3H, $CH_{3\text{-}Mes}$); 2.04 (s, 3H, $CH_{3\text{-}Mes}$); 1.22 (s, 3H, $CH_{3\text{-}Mes}$); 0.98 (t, $^3J_{HH}$ = 7.2 Hz, 6H, NCH$_2$CH_3), -8.41 (dd, $^2J_{HP}$ = 34.4 Hz, $^2J_{HP}$ = 77.4 Hz, 1H, RuH). ^{13}C{^{1}H}n2o NMR (CD_2Cl_2): δ 207.60 (dd, $^2J_{CP}$ = 80.4 Hz, $^2J_{CP}$ = 6.0 Hz, C_{NHC}); 204.50 (dd, $^2J_{CP}$ = 13.2 Hz, $^2J_{CP}$ = 6.7 Hz, C_{CO}); 162.40 (t, $^3J_{CP}$ = 2.6 Hz, C_{pyr}); 151.91 (dd, $^2J_{CP}$ = 9.9 Hz, $^2J_{CP}$ = 15.2 Hz, C_{pyr}); 151.64 (t, $^3J_{CP}$ = 3.8 Hz, C_{pyr}); 150.70 (s, C_{pyr}); 139.30 (s, C_{Mes}); 138.47 (dd, $^2J_{CP}$ = 35.0 Hz, $^3J_{CP}$ = 1.6 Hz, C_{PPh3}); 138.26 (s, C_{Mes}); 137.06 (dd, $^2J_{CP}$ = 29.1 Hz, $^3J_{CP}$ = 1.3 Hz, C_{PPh3}); 136.74 (s, C_{Mes}); 136.68 (d, $^4J_{CP}$ = 3.2, $C_{benzimid}$); 134.33 (d, $^2J_{CP}$ = 10.9 Hz, C_{PPh3}); 133.78 (s, C_{Mes}); 133.30 (d, $^2J_{CP}$ = 11.0 Hz, C_{PPh3}); 132.08 (d, $^4J_{CP}$ = 1.7, $C_{benzimid}$); 129.54 (s, C_{Mes}); 128.72 (s, C_{Mes}); 128.64 (s, C_{PPh3}); 128.52 (s, C_{PPh3}); 127.32 (d, $^3J_{CP}$ = 8.6 Hz, two *meta* C_{PPh3} peaks overlapped); 122.32 (s, $C_{benzimid}$); 122.24 (s, $C_{benzimid}$); 117.34 (s, C_{pyr}); 113.90 (s, $C_{benzimid}$); 108.90 (s, $C_{benzimid}$); 58.61 (s, *C*H$_2$NEt$_2$); 46.91 (s, N*C*H$_2$CH$_3$); 20.92 (s, $CH_{3\text{-}Mes}$); 18.33 (s, $CH_{3\text{-}Mes}$); 16.91 (s, $CH_{3\text{-}Mes}$); 12.00 (s, NCH$_2$*C*H$_3$). ^{31}P{^{1}H} NMR (CD_2Cl_2): δ 46.83 (d, $^2J_{PP}$ = 21.6 Hz); 31.08 (d, $^2J_{PP}$ = 21.6 Hz). Anal calcd. for $C_{63}H_{60}N_4OP_2Ru$: C, 71.91; H, 5.75; N, 5.32. Found: C, 71.50; H, 5.68; N, 5.26.

***cis*-Ru-dipp-Et-PPh$_3$**. In the glove box, **Ru-dipp-Et** (50 mg, 0.082 mmol), a stir bar, triphenylphosphine (130 mg, 0.50 mmol), NaO^{t}Bu (48 mg, 0.50 mmol), and toluene (5 mL) were added to a vial and stirred overnight at room temperature. A short silica gel column was performed in the glovebox using a 6 mL plastic syringe and a PTFE filter disk. The crude product was loaded with toluene and impurities were washed away with dichloromethane (ca. 15 mL). The product was then eluted with THF (ca. 10 mL). The resulting green film after evaporation of THF was dissolved in benzene and frozen. A green powder was obtained after sublimation of benzene. Yield: 65 mg, 79%. ^{1}H NMR (CD_2Cl_2): δ 8.82 (d, $^3J_{HH}$ = 8.0 Hz, 1H, $CH_{benzimid}$); 7.27 (t, $^3J_{HH}$ = 7.7 Hz, 1H, CH_{dipp}); 7.26-7.20 (m, 7H, CH_{dipp} and CH_{PPh3}); 7.13 (t, 2H, $^3J_{HH}$ = 7.2 Hz, $CH_{benzimid}$); 7.06 (d, $^3J_{HH}$ = 8.0 Hz, 1H, CH_{dipp}); 7.05-6.92 (m, 7H, CH_{PPh3} and $CH_{benzimid}$); 6.88 (m, 6H, CH_{PPh3}); 6.79 (m, 6H, CH_{PPh3}); 6.63-6.58 (m, 7H, CH_{PPh3} and CH_{pyr}); 6.45 (d, $^3J_{HH}$ = 8.0 Hz, 1H, $CH_{benzimid}$); 6.12 (d, $^3J_{HH}$ = 7.4 Hz, 1H, CH_{pyr}); 3.52 (AB pattern, $^2J_{HH}$ = 13.7 Hz, 2H, CH_2NEt$_2$); 2.40 (q, $^3J_{HH}$ = 7.0 Hz, 4H, NCH_2CH$_3$); 2.15 (sept, $^3J_{HH}$ = 6.8 Hz, 1H, CH_{iPr}); 2.09 (sept, $^3J_{HH}$ = 6.8 Hz, 1H, CH_{iPr}); 0.93 (t, $^3J_{HH}$ = 7.0 Hz, 6H, NCH$_2$CH_3); 0.83 (d, $^3J_{HH}$ = 6.8 Hz, 3H, $CH_{3\text{-}iPr}$); 0.58 (d, $^3J_{HH}$ = 6.8 Hz, 3H, $CH_{3\text{-}iPr}$); 0.50 (d, $^3J_{HH}$ = 6.8 Hz, 3H, $CH_{3\text{-}iPr}$); 0.48 (d, $^3J_{HH}$ = 6.8 Hz, 3H, $CH_{3\text{-}iPr}$); -8.79 (dd, $^2J_{HP}$ = 32.3 Hz, $^2J_{HP}$ = 76.1 Hz, 1H, RuH). ^{13}C NMR (CD_2Cl_2): δ 209.98 (dd, $^2J_{CP}$ = 80.4 Hz, $^2J_{CP}$ = 5.7 Hz, C_{NHC}); 204.65 (dd, $^2J_{CP}$ = 10.6 Hz, $^2J_{CP}$ = 7.1 Hz, C_{CO}); 162.02 (t, $^3J_{CP}$ = 3.0 Hz, C_{pyr}); 153.62 (dd, $^2J_{CP}$ = 10.4 Hz, $^2J_{CP}$ = 15.3 Hz, C_{pyr}); 153.22 (dd, $^3J_{CP}$ = 6.1 Hz, $^3J_{CP}$ = 2.6 Hz, C_{pyr}); 150.72 (s, C_{pyr}); 148.57 (s, C_{dipp}); 147.30 (s, C_{dipp}); 139.26 (d, $^4J_{CP}$ = 3.4 Hz, $C_{benzimid}$); 138.66 (dd, $^1J_{CP}$ = 34.5 Hz, $^3J_{CP}$ = 1.8 Hz, C_{PPh3}); 137.56 (d, $^1J_{CP}$ = 28.4 Hz, C_{PPh3}); 134.51 (s, C_{dipp}); 134.26 (d, $^2J_{CP}$ = 11.0 Hz, C_{PPh3}); 133.25 (d, $^2J_{CP}$ = 11.2 Hz, C_{PPh3}); 132.06 (d, $^4J_{CP}$ = 1.9 Hz, $C_{benzimid}$); 129.74 (s, C_{dipp}); 128.50 (s, C_{PPh3}); 128.45 (s, C_{PPh3}); 127.40 (d, $^3J_{CP}$ = 8.5 Hz, C_{PPh3}); 127.26 (d, $^3J_{CP}$ = 8.8 Hz, C_{PPh3}); 124.68 (s, C_{dipp}); 123.70 (s, C_{dipp}); 122.38 (s, $C_{benzimid}$); 121.77 (s, $C_{benzimid}$); 117.63 (s, C_{pyr}); 113.77 (s, $C_{benzimid}$); 110.91 (s, $C_{benzimid}$); 58.73 (s, *C*H$_2$NEt$_2$); 46.94 (s, N*C*H$_2$CH$_3$); 28.26 (s, CH_{iPr}); 28.22 (s, CH_{iPr}); 24.96 (s, $CH_{3\text{-}iPr}$); 24.90 (s, $CH_{3\text{-}iPr}$); 23.10 (s, $CH_{3\text{-}iPr}$); 22.65 (s, $CH_{3\text{-}iPr}$); 12.02 (s, NCH$_2$*C*H$_3$). ^{31}P{^{1}H} NMR (CD_2Cl_2): δ 44.87 (d, $^2J_{PP}$ = 21.8 Hz); 27.98 (d, $^2J_{PP}$ = 21.8 Hz). Anal. calcd. for $C_{66}H_{66}N_4OP_2Ru$: C, 72.44; H, 6.08; N, 5.12. Found: C, 72.50; H, 6.27; N, 4.90.

***trans*-Ru-Mes-Et-PPh$_3$**. In the glove box, **Ru-Mes-Et** (96 mg, 0.170 mmol), a stir bar, triphenylphosphine (267 mg, 1.02 mmol), NaO^{t}Bu (98 mg, 1.02 mmol), and toluene (10 mL) were added to a vial and stirred overnight at 80 °C. The crude reaction mixture was then purified by air-free gradient flash chromatography, using a gradient of 0 to 100% ethyl acetate in dichloromethane. Yield: 106 mg, 59%. ^{1}H NMR (CD_2Cl_2): δ 8.72 (d, $^3J_{HH}$ = 8.0 Hz, 1H, $CH_{benzimid}$); 7.17 (t, $^3J_{HH}$ = 7.7 Hz, 1H, $CH_{benzimid}$); 7.12-7.07 (m, 6H, CH_{PPh3}); 7.04-6.95 (m, 25H, CH_{PPh3} and $CH_{benzimid}$); 6.89 (s, 2H, CH_{Mes}); 6.53 (d, $^3J_{HH}$ = 8.0 Hz, 1H, $CH_{benzimid}$); 6.33 (dt, $^3J_{HH}$ = 7.4 Hz, $^4J_{HP}$ = 1.2 Hz, 1H, CH_{pyr}); 6.08 (d, $^3J_{HH}$ = 7.4 Hz, 1H, CH_{pyr}); 3.52 (s, 2H, CH_2NEt$_2$); 2.43 (q, $^3J_{HH}$ = 7.1 Hz, 4H, NCH_2CH$_3$); 2.34 (s, 3H, $CH_{3\text{-}Mes}$); 1.18 (s, 6H, $CH_{3\text{-}Mes}$) 0.96 (t, $^3J_{HH}$ = 7.1 Hz, 6H, NCH$_2$CH_3); -7.07 (t, $^2J_{HP}$ = 28.2 Hz, RuH). ^{13}C{^{1}H} NMR (CD_2Cl_2): δ 212.88 (t, $^2J_{CP}$ = 5.7 Hz, C_{NHC}); 206.36 (t, $^2J_{CP}$ = 10.1 Hz, C_{CO}); 163.18 (t, $^3J_{CP}$ = 2.2 Hz, C_{pyr}); 152.36 (s, C_{pyr}); 151.09 ($^2J_{CP}$ = 17.3 Hz, C_{pyr}); 150.72 (s, C_{pyr}); 138.81 (s, C_{dipp}); 137.26 (t, $^1J_{CP}$ = 21.5 Hz, C_{PPh3}); 137.26 (s, C_{dipp}); 137.09 (s, $C_{benzimid}$); 134.33 (s, C_{dipp}); 133.52 (t, $^2J_{CP}$ = 5.9 Hz, C_{PPh3}); 132.78 (s, $C_{benzimid}$); 128.98 (s, C_{dipp}); 128.64 (s, C_{PPh3}); 127.19 (t, $^3J_{CP}$ = 4.5 Hz, C_{PPh3}); 122.11 (s, $C_{benzimid}$); 121.86 (s, $C_{benzimid}$); 118.14 (s, C_{pyr}); 114.39 (s, $C_{benzimid}$); 108.67 (s, $C_{benzimid}$); 58.27 (s, *C*H$_2$NEt$_2$); 46.88 (s, N*C*H$_2$CH$_3$); 20.89 (s, $CH_{3\text{-}Mes}$); 17.43 (s, $CH_{3\text{-}Mes}$); 12.03 (s, NCH$_2$*C*H$_3$). ^{31}P{^{1}H} NMR (CD_2Cl_2): δ 51.24 (s). Anal. calcd. for $C_{63}H_{60}N_4OP_2Ru$: C, 71.91; H, 5.75; N, 5.32. Found: C, 71.88; H, 5.87; N, 5.04.

Ru-Mes-Et-PCy$_3$. In the glove box, **Ru-Mes-Et** (50 mg, 0.89 mmol), a stir bar, tricyclohexylphosphine (149 mg, 0.532 mmol), NaO^{t}Bu (51 mg, 0.53 mmol), and toluene (7 mL) were

added to a vial and stirred overnight at room temperature. The crude reaction mixture was purified by air-free gradient flash chromatography, using a gradient of 0 to 100% ethyl acetate in dichloromethane. The residue was then recrystallized by layering acetonitrile over a concentrated dichloromethane solution in the glove box. The colorless solid formed was washed with a 6:1 mixture of acetonitrile to dichloromethane, then dried under vacuum. Yield: 41 mg, 43%. ^{1}H NMR (CD_2Cl_2): δ 8.94 (d, $^{3}J_{HH}$ = 7.9 Hz, 1H, $CH_{benzimid}$); 7.81 (d, $^{3}J_{HH}$ = 7.2 Hz, 1H, CH_{pyr}); 7.13 (t, $^{3}J_{HH}$ = 7.9 Hz, 1H, $CH_{benzimid}$); 7.00 (t, $^{3}J_{HH}$ = 7.9 Hz, 1H, $CH_{benzimid}$); 6.94 (s, 2H, CH_{Mes}); 6.76 (d, $^{3}J_{HH}$ = 7.2 Hz, 1H, CH_{pyr}); 6.51 (d, $^{3}J_{HH}$ = 7.9 Hz, 1H, $CH_{benzimid}$); 3.67 (s, 2H, CH_2NEt_2); 2.55 (q, $^{3}J_{HH}$ = 7.2 Hz, 4H, NCH_2CH_3); 2.28 (s, 3H, $CH_{3\text{-}Mes}$); 1.99 (br s, 6H, $CH_{3\text{-}Mes}$); 1.87-0.72 (br m, 66H, CH_{PCy3}); 1.02 (t, $^{3}J_{HH}$ = 7.2 Hz, 6H, NCH_2CH_3); -8.25 (t, $^{2}J_{HP}$ = 31.7 Hz, RuH). ^{13}C NMR (CD_2Cl_2): δ 217.78 (t, $^{2}J_{CP}$ = 4.4 Hz, C_{NHC}); 207.88 (t, $^{2}J_{CP}$ = 11.2 Hz, C_{CO}); 163.00 (s, C_{pyr}); 157.52 (t, $^{2}J_{CP}$ = 14.4 Hz, C_{pyr}); 152.82 (s, C_{pyr}); 150.21 (s, C_{pyr}); 138.63 (s, $C_{benzimid}$); 137.78 (s, C_{Mes}); 137.10 (s, C_{dipp}); 134.78 (s, C_{Mes}); 132.95 ($C_{benzimid}$); 129.43 (s, C_{Mes}); 121.70 (s, C_{Mes}); 121.58 (s, C_{Mes}); 118.05 (s, C_{pyr}); 113.77 (s, $C_{benzimid}$); 108.84 (s, $C_{benzimid}$); 58.92 (s, CH_2NEt_2); 46.68 (s, NCH_2CH_3); 37.32 (br s, C_{PCy3}); 29.87 (br s, C_{PCy3}); 29.67 (br s, C_{PCy3}); 28.00-27.75 (br m, C_{PCy3}); 26.75 (s, C_{PCy3}); 20.72 (s, $CH_{3\text{-}Mes}$); 19.69 (br s, $CH_{3\text{-}Mes}$); 11.94 (s, NCH_2CH_3). ^{31}P{^{1}H} NMR (CD_2Cl_2): δ 48.13 (br s). ^{1}H NMR (CD_2Cl_2, 220 K, hydride region): δ -8.09 (br). ^{31}P{^{1}H} NMR (CD_2Cl_2, 220 K): δ 51.4 (d, $^{2}J_{PP}$ = 195 Hz); 44.4 (d, $^{2}J_{PP}$ = 195 Hz). Anal. calcd. for $C_{63}H_{96}N_4OP_2Ru$: C, 69.52; H, 8.89; N, 5.15. Found: C, 68.63; H, 8.72; N, 5.10. Although this complex appeared pure by NMR, a more satisfactory analysis could not be obtained.

Ru-dipp-Me-PCy$_3$. In the glove box, **Ru-dipp-Me** (50 mg, 0.87 mmol), a stir bar, tricyclohexylphosphine (146 mg, 0.519 mmol), NaO^{t}Bu (50 mg, 0.52 mmol), and toluene (7 mL) were added to a vial and stirred overnight at room temperature. As NMR showed the reaction was not complete, the solution was heated at 80 °C for three hours. The crude reaction mixture was then purified by air-free gradient flash chromatography, using a gradient of 0 to 100% ethyl acetate in dichloromethane. The residue was then recrystallized by layering acetonitrile over a concentrated dichloromethane solution in the glove box. The colorless solid formed was washed with a 6:1 mixture of acetonitrile to dichloromethane, then dried under vacuum. Yield: 21 mg, 25%. ^{1}H NMR (C_6D_6): δ 9.51 (d, $^{3}J_{HH}$ = 8.0 Hz, 1H, $CH_{benzimid}$); 8.24 (d, $^{3}J_{HH}$ = 7.2 Hz, 1H, CH_{pyr}); 7.37-7.30 (br, 3H, CH_{dipp}); 7.22 (d, $^{3}J_{HH}$ = 7.2 Hz, 1H, CH_{pyr}); 7.14 (t, $^{3}J_{HH}$ = 8.0 Hz, 1H, $CH_{benzimid}$); 6.86 (t, $^{3}J_{HH}$ = 8.0 Hz, 1H, $CH_{benzimid}$); 6.73 (d, $^{3}J_{HH}$ = 8.0 Hz, 1H, $CH_{benzimid}$); 3.82 (s, 2H, CH_2NMe_2); 2.37 (s, 6H, $N(CH_3)_2$), 2.11-0.25 (br m, 78H, CH_{PCy3} and $CH_{3\text{-}dipp}$); -8.21 (t, $^{2}J_{HP}$ = 31.6 Hz, RuH). ^{13}C NMR (C_6D_6): δ 220.71 (t, $^{2}J_{CP}$ = 4.7 Hz, C_{NHC}); 268.01 (t, $^{2}J_{CP}$ = 11.2 Hz, C_{CO}); 164.06 (t, $^{3}J_{CP}$ = 2.0 Hz, C_{pyr}); 158.10 (t, $^{2}J_{CP}$ = 14.1 Hz, C_{pyr}); 153.17 (s, C_{pyr}); 150.95 (s, C_{pyr}); 148.07 (s, C_{dipp}); 141.14 (s, $C_{benzimid}$); 136.72 (s, C_{dipp}); 133.47 (s, $C_{benzimid}$); 129.84 (s, C_{dipp}); 124.89 (br s, C_{dipp}); 122.56 (s, $C_{benzimid}$); 121.59 (s, $C_{benzimid}$); 118.35 (s, C_{pyr}); 114.81 (s, $C_{benzimid}$); 112.44 (s, $C_{benzimid}$); 66.57 (s, CH_2NMe_2); 46.57 (s, $N(CH_3)_2$); 37.00 (br s, C_{PCy3}); 30.36 (br s, C_{PCy3}); 29.07 (br s, C_{dipp}); 28.27 (br s, C_{PCy3}); 27.21 (br s, C_{PCy3}); 26.85 (br s, C_{dipp}); 23.83 (br s, C_{dipp}). ^{31}P{^{1}H} NMR (CD_2Cl_2): δ 46.71 (br s).). ^{1}H NMR (CD_2Cl_2, 220 K, hydride region): δ -8.45 (dd, $^{2}J_{HP}$ = 26.9, 35.0 Hz). ^{31}P{^{1}H} NMR (CD_2Cl_2, 220 K): 50.9 (d, $^{2}J_{PP}$ = 203 Hz); 42.1 (d, $^{2}J_{PP}$ = 203 Hz). Anal. calcd. for $C_{64}H_{98}N_4OP_2Ru$: C, 69.72; H, 8.96; N, 5.08. Found: 70.31; H, 8.82; N, 4.53.

Ru-dipp-Et-PCy$_3$. In the glove box, **Ru-dipp-Et** (63 mg, 0.104 mmol), a stir bar, tricyclohexylphosphine (175 mg, 0.624 mmol), NaO^{t}Bu (60 mg, 0.62 mmol), and toluene (5 mL) were added to a vial and stirred overnight at room temperature. The crude reaction mixture was then purified by air-free gradient flash chromatography, using a gradient of 0 to 100% ethyl acetate in dichloromethane. The residue was then recrystallized by layering acetonitrile over a concentrated dichloromethane solution in the glove box. The colorless solid formed was washed with a 6:1 mixture of acetonitrile to dichloromethane, then dried under vacuum. Yield: 41 mg, 35%. ^{1}H NMR (CD_2Cl_2): δ 8.92 (d, $^{3}J_{HH}$ = 8.0 Hz, 1H, $CH_{benzimid}$); 7.81 (d, $^{3}J_{HH}$ = 7.2 Hz, 1H, CH_{pyr}); 7.25 (t, $^{3}J_{HH}$ = 7.8 Hz, 2H, CH_{dipp}); 7.25 (d, $^{3}J_{HH}$ = 7.8 Hz, 1H, CH_{dipp}); 7.14 (t, $^{3}J_{HH}$ = 8.0 Hz, 1H, $CH_{benzimid}$); 6.99 (t, $^{3}J_{HH}$ = 8.0 Hz, 1H, $CH_{benzimid}$); 6.78 (d, $^{3}J_{HH}$ = 7.2 Hz, 1H, CH_{pyr}); 6.69 (d, $^{3}J_{HH}$ = 8.0 Hz, 1H, $CH_{benzimid}$); 3.66 (s, 2H, CH_2NMe_2); 2.53 (q, $^{3}J_{HH}$ = 7.2 Hz, 4H, NCH_2CH_3); 2.0-0.0 (br m, 78H, CH_{PCy3} and $CH_{3\text{-}dipp}$); 1.02 (t, $^{3}J_{HH}$ = 7.2 Hz, 6H, NCH_2CH_3); -8.55 (t, $^{2}J_{HP}$ = 31.6 Hz, RuH). ^{13}C NMR (CD_2Cl_2): δ 220.91 (t, $^{2}J_{CP}$ = 4.7 Hz, C_{NHC}); 208.08 (t, $^{2}J_{CP}$ = 11.3 Hz, C_{CO}); 163.61 (s, C_{pyr}); 157.90 (t, $^{2}J_{CP}$ = 14.3 Hz, C_{pyr}); 153.17 (s, C_{pyr}); 150.79 (s, C_{pyr}); 148.11 (s, C_{dipp}); 141.01 (s, $C_{benzimid}$); 136.48 (s, C_{dipp}); 133.31 (s, $C_{benzimid}$); 129.74 (s, C_{dipp}); 124.73 (br s, C_{dipp}); 122.17 (s, $C_{benzimid}$); 121.28 (s, $C_{benzimid}$); 118.57 (s, C_{pyr}); 114.06 (s, $C_{benzimid}$); 112.50 (s, $C_{benzimid}$); 59.49 (s, CH_2NEt_2); 47.17 (s, $N(CH_2CH_3)_2$); 36.95 (br s, C_{PCy3}); 30.12 (br s, C_{PCy3}); 29.01 (br s, C_{dipp}); 28.24 (br s, C_{PCy3}); 27.13 (br s, C_{PCy3}); 26.68 (br s, C_{dipp}); 23.64 (br s, C_{dipp}); 12.42 (s, $N(CH_2CH_3)_2$). ^{31}P{^{1}H} NMR (CD_2Cl_2): δ 45.37 (br s). ^{1}H NMR (CD_2Cl_2, 220 K, hydride region): δ -8.46 (br dd). ^{31}P{^{1}H} NMR (CD_2Cl_2, 220 K): 51.2 (d, $^{2}J_{PP}$ = 206 Hz); 42.2 (d, $^{2}J_{PP}$ = 206 Hz). Anal. calcd. for $C_{66}H_{102}N_4OP_2Ru$: C, 70.12; H, 9.09; N, 4.96. Found: C, 70.03; H, 8.94; N, 4.88.

Ru-dipp-^{i}Pr-PCy$_3$. In the glove box, **Ru-dipp-^{i}Pr** (50 mg, 0.079 mmol), a stir bar, tricyclohexylphosphine (133 mg, 0.473 mmol), NaO^{t}Bu (46 mg, 0.47 mmol), and toluene (7 mL) were added to a vial and stirred overnight at room temperature. The crude reaction mixture was then purified by air-free gradient flash chromatography, using a gradient of 0 to 100% ethyl acetate in dichloromethane. The residue was recrystallized in the glovebox by layering acetonitrile over a concentrated solution in dichloromethane. The colorless solid formed was washed with a 6:1 mixture of acetonitrile to dichloromethane, then dried under vacuum. Yield: 33 mg, 37%. ^{1}H NMR (CD_2Cl_2): δ 8.96 (d, $^{3}J_{HH}$ = 8.0 Hz, 1H, $CH_{benzimid}$); 7.79 (d, $^{3}J_{HH}$ = 7.2 Hz, 1H, CH_{pyr}); 7.34 (t, $^{3}J_{HH}$ = 7.8 Hz, 2H, CH_{dipp}); 7.25 (t, $^{3}J_{HH}$ = 7.8 Hz, 2H, CH_{dipp}); 7.13 (t, $^{3}J_{HH}$ = 8.0 Hz, 1H, $CH_{benzimid}$); 7.00 (t, $^{3}J_{HH}$ = 8.0 Hz, 1H, $CH_{benzimid}$); 6.96 7.79 (d, $^{3}J_{HH}$ = 7.2 Hz, 1H, CH_{pyr}); 6.69 (d, $^{3}J_{HH}$ = 8.0 Hz, 1H, $CH_{benzimid}$); 3.70 (s, 2H, $NCH_2{}^{i}Pr$); 3.04 (sept, $^{3}J_{HH}$ = 6.6 Hz, 2H, CH_{iPr}); 2.0-0.0 (br m, 78H, CH_{PCy3} and $CH_{3\text{-}dipp}$); 0.99 (d, $^{3}J_{HH}$ = 6.6 Hz, 12H, $CH_{3\text{-}iPr}$); -8.58 (t, $^{2}J_{HP}$ = 31.6 Hz, RuH). ^{13}C NMR (CD_2Cl_2): δ 220.37 (t, $^{2}J_{CP}$ = 4.7 Hz, C_{NHC}); 207.63 (t, $^{2}J_{CP}$ = 11.3 Hz, C_{CO}); 162.77 (t, $^{3}J_{CP}$ = 2.0 Hz, C_{pyr}); 156.00 (t, $^{2}J_{CP}$ = 14.6 Hz, C_{pyr}); 154.54 (s, C_{pyr}); 152.84 (s, C_{pyr}); 147.69 (s, C_{dipp}); 140.57 (s, $C_{benzimid}$); 136.09 (s, C_{dipp}); 132.93 (s, $C_{benzimid}$); 129.26 (s, C_{dipp}); 124.29 (br s, C_{dipp}); 121.68 (s, $C_{benzimid}$); 120.76 (s, $C_{benzimid}$); 117.13 (s, C_{pyr}); 113.70 (s, $C_{benzimid}$); 112.01 (s, $C_{benzimid}$); 51.22 (s, $CH_2N{}^{i}Pr_2$); 48.35 (s, $N(CH_2(CH_3)_2)_2$); 36.21 (br s, C_{PCy3}); 29.70 (br s, C_{PCy3}); 28.56 (br s, C_{dipp}); 27.82 (br s, C_{PCy3}); 26.71 (br s, C_{PCy3}); 26.25 (br s, C_{dipp}); 23.19 (br s, C_{dipp}); 20.56 (s, $N(CH_2(CH_3)_2)_2$). ^{31}P{^{1}H} NMR (CD_2Cl_2): δ 47.44 (br m). ^{1}H NMR (CD_2Cl_2, 220 K, hydride region): δ -8.48 (dd, $^{2}J_{HP}$ = 27.0, 34.8 Hz). ^{31}P{^{1}H} NMR (CD_2Cl_2, 220 K): 51.0 (d, $^{2}J_{PP}$

= 204 Hz); 42.2 (d, $^2J_{PP}$ = 204 Hz). Anal. calcd. for $C_{68}H_{106}N_4OP_2Ru$: C, 70.49; H, 9.22; N, 4.84. Found: C, 70.15; H, 8.83; N, 4.85.

General Procedure for Ester Hydrogenation. In an argon-filled glovebox, the ruthenium complex, ester, and tetradecane as internal standard were dissolved in toluene and transferred to a test tube containing a stir bar. The tube was placed in a stainless-steel pressure reactor inside the glovebox, which was subsequently sealed and brought out. Then, the reactor was pressurized with 30 bar H_2 and vented three times to remove the argon atmosphere, and finally it was filled with 30 bar H_2. The reactor was heated at 105 °C while stirring for 20 hours, after which it was allowed to cool for 1 h before being vented carefully and opened. An aliquot of the reaction mixture was taken and analyzed by GC-FID. Yields were calculated based on the calibrated response factors of the product(s) relative to the tetradecane standard.

Computational Details. All density functional theory calculations were performed using the Gaussian 16 computational chemistry package, Revision B.01.[25] The geometries and energies of all species were calculated using the hybrid functional B3LYP,[26] augmented with the addition of empirical dispersion with Grimme's D3 dispersion corrections[27] (referred to as B3LYP-d3). Ru was modeled with the effective core potential of Hay and Wadt[28] and the accompanying uncontracted basis set (including f polarization functions)[29] collectively known as LANL08(f).[30] All other elements were modeled with the 6-311G(d,p) basis set.[31] Complete structures with no truncations were used in all cases, and were optimized in the gas phase. Frequency calculations ensured the absence of imaginary vibrational modes for intermediates and exactly one for transition states. Transition states were confirmed to lead to the intermediates shown using intrinsic reaction coordinate calculations. Solvent corrections were added with a polarizable continuum model with radii and non-electrostatic terms from Truhlar and coworkers' SMD solvation model, and with dielectric constants chosen for toluene.[32] Standard state corrections were added in order to adjust from 1 atm to 1 M for solution-phase free energies.[33]

ASSOCIATED CONTENT

Supporting Information

The Supporting Information is available free of charge on the ACS Publications website at DOI: xxx.

Experimental procedures for X-ray crystallography, images of NMR spectra and detailed NMR assignments for new compounds, and additional details of computational studies (PDF). Atomic coordinates and energies for all computed molecular structures, compiled as one file readable by the free program Mercury[34] (XYZ).

AUTHOR INFORMATION

Corresponding Author

*E-mail: achianese@colgate.edu

Notes

The authors declare no competing financial interest.

ACKNOWLEDGEMENTS

We thank the National Science Foundation (CHE-1665144) for support of the research project, and (CHE-1726308) for the acquisition of an upgraded NMR spectrometer.

REFERENCES

(1) Zhang, J.; Leitus, G.; Ben-David, Y.; Milstein, D. Efficient Homogeneous Catalytic Hydrogenation of Esters to Alcohols. *Angew. Chem. Int. Ed.* **2006,** *45*, 1113-1115.

(2) Zhang, J.; Leitus, G.; Ben-David, Y.; Milstein, D. Facile Conversion of Alcohols into Esters and Dihydrogen Catalyzed by New Ruthenium Complexes. *J. Am. Chem. Soc.* **2005,** *127*, 10840-10841.

(3) Blum, Y.; Czarkie, D.; Rahamim, Y.; Shvo, Y. (Cyclopentadienone)Ruthenium Carbonyl Complexes - a New Class of Homogeneous Hydrogenation Catalysts. *Organometallics* **1985,** *4*, 1459-1461.

(4) Noyori, R.; Ohkuma, T. Asymmetric Catalysis by Architectural and Functional Molecular Engineering: Practical Chemo- and Stereoselective Hydrogenation of Ketones. *Angew. Chem. Int. Ed.* **2001,** *40*, 40-73.

(5) (a) Tan, X.; Wang, Y.; Liu, Y.; Wang, F.; Shi, L.; Lee, K. H.; Lin, Z.; Lv, H.; Zhang, X. Highly Efficient Tetradentate Ruthenium Catalyst for Ester Reduction: Especially for Hydrogenation of Fatty Acid Esters. *Org. Lett.* **2015,** *17*, 454-457. (b) Tan, X.; Wang, Q.; Liu, Y.; Wang, F.; Lv, H.; Zhang, X. A New Designed Hydrazine Group-Containing Ruthenium Complex Used for Catalytic Hydrogenation of Esters. *Chem. Commun.* **2015,** *51*, 12193-12196. (c) Spasyuk, D.; Vicent, C.; Gusev, D. G. Chemoselective Hydrogenation of Carbonyl Compounds and Acceptorless Dehydrogenative Coupling of Alcohols. *J. Am. Chem. Soc.* **2015,** *137*, 3743-3746. (d) Filonenko, G. A.; Aguila, M. J. B.; Schulpen, E. N.; van Putten, R.; Wiecko, J.; Müller, C.; Lefort, L.; Hensen, E. J. M.; Pidko, E. A. Bis-N-Heterocyclic Carbene Aminopincer Ligands Enable High Activity in Ru-Catalyzed Ester Hydrogenation. *J. Am. Chem. Soc.* **2015,** *137*, 7620-7623. (e) Li, W.; Xie, J.-H.; Yuan, M.-L.; Zhou, Q.-L. Ruthenium Complexes of Tetradentate Bipyridine Ligands: Highly Efficient Catalysts for the Hydrogenation of Carboxylic Esters and Lactones. *Green Chem.* **2014,** *16*, 4081-4085. (f) Spasyuk, D.; Smith, S.; Gusev, D. G. Replacing Phosphorus with Sulfur for the Efficient Hydrogenation of Esters. *Angew. Chem. Int. Ed.* **2013,** *52*, 2538-2542. (g) Spasyuk, D.; Gusev, D. G. Acceptorless Dehydrogenative Coupling of Ethanol and Hydrogenation of Esters and Imines. *Organometallics* **2012,** *31*, 5239-5242. (h) Saudan, L. A.; Saudan, C. M.; Debieux, C.; Wyss, P. Dihydrogen Reduction of Carboxylic Esters to Alcohols under the Catalysis of Homogeneous Ruthenium Complexes: High Efficiency and Unprecedented Chemoselectivity. *Angew. Chem. Int. Ed.* **2007,** *46*, 7473-7476.

(6) (a) Takebayashi, S.; Bergens, S. H. Facile Bifunctional Addition of Lactones and Esters at Low Temperatures. The First Intermediates in Lactone/Ester Hydrogenations. *Organometallics* **2009,** *28*, 2349-2351. (b) Werkmeister, S.; Junge, K.; Wendt, B.; Alberico, E.; Jiao, H.; Baumann, W.; Junge, H.; Gallou, F.; Beller, M. Hydrogenation of Esters to Alcohols with a Well-Defined Iron Complex. *Angew. Chem. Int. Ed.* **2014,** *53*, 8722-8726. (c) Brewster, T. P.; Rezayee, N. M.; Culakova, Z.; Sanford, M. S.; Goldberg, K. I. Base-Free Iridium-Catalyzed Hydrogenation of Esters and Lactones. ACS Catal. 2016, 6, 3113-3117. (d) Gusev, D. G. Dehydrogenative Coupling of Ethanol and Ester Hydrogenation Catalyzed by Pincer-Type Ynp Complexes. ACS Catal. 2016, 6, 6967-6981. (e) Espinosa-Jalapa, N. A.; Nerush, A.; Shimon, L. J. W.; Leitus, G.; Avram, L.; Ben-David, Y.; Milstein, D. Manganese-Catalyzed Hydrogenation of Esters to Alcohols. Chem. Eur. J. 2017, 23, 5934-5938. (f) van Putten, R.; Uslamin, E. A.; Garbe, M.; Liu, C.; Gonzalez-de-Castro, A.; Lutz, M.; Junge, K.; Hensen, E. J. M.; Beller, M.; Lefort, L.; Pidko, E. A. Non-Pincer-Type Manganese Complexes as Efficient Catalysts for the Hydrogenation of Esters.

Angew. Chem. Int. Ed. **2017,** *56*, 7531-7534. (g) Yuwen, J.; Chakraborty, S.; Brennessel, W. W.; Jones, W. D. Additive-Free Cobalt-Catalyzed Hydrogenation of Esters to Alcohols. *ACS Catal.* **2017,** *7*, 3735-3740. (h) Junge, K.; Wendt, B.; Cingolani, A.; Spannenberg, A.; Wei, Z.; Jiao, H.; Beller, M. Cobalt Pincer Complexes for Catalytic Reduction of Carboxylic Acid Esters. *Chem. Eur. J.* **2018,** *24*, 1046-1052.

(7) (a) Hasanayn, F.; Baroudi, A. Direct H/OR and OR/OR′ Metathesis Pathways in Ester Hydrogenation and Transesterification by Milstein's Catalyst. *Organometallics* **2013,** *32*, 2493-2496. (b) O, W. W. N.; Morris, R. H. Ester Hydrogenation Catalyzed by a Ruthenium(II) Complex Bearing an N-Heterocyclic Carbene Tethered with an "NH_2" Group and a DFT Study of the Proposed Bifunctional Mechanism. *ACS Catal.* **2013,** *3*, 32-40. (c) Otsuka, T.; Ishii, A.; Dub, P. A.; Ikariya, T. Practical Selective Hydrogenation of Alpha-Fluorinated Esters with Bifunctional Pincer-Type Ruthenium(II) Catalysts Leading to Fluorinated Alcohols or Fluoral Hemiacetals. *J. Am. Chem. Soc.* **2013,** *135*, 9600-9603. (d) Chakraborty, S.; Lagaditis, P. O.; Förster, M.; Bielinski, E. A.; Hazari, N.; Holthausen, M. C.; Jones, W. D.; Schneider, S. Well-Defined Iron Catalysts for the Acceptorless Reversible Dehydrogenation-Hydrogenation of Alcohols and Ketones. *ACS Catal.* **2014,** *4*, 3994-4003. (e) Chen, T.; Li, H.; Qu, S.; Zheng, B.; He, L.; Lai, Z.; Wang, Z.-X.; Huang, K.-W. Hydrogenation of Esters Catalyzed by Ruthenium PN_3-Pincer Complexes Containing an Aminophosphine Arm. *Organometallics* **2014,** *33*, 4152-4155. (f) Junge, K.; Wendt, B.; Jiao, H.; Beller, M. Iridium-Catalyzed Hydrogenation of Carboxylic Acid Esters. *ChemCatChem* **2014,** *6*, 2810-2814. (g) Qu, S.; Dai, H.; Dang, Y.; Song, C.; Wang, Z.-X.; Guan, H. Computational Mechanistic Study of Fe-Catalyzed Hydrogenation of Esters to Alcohols: Improving Catalysis by Accelerating Precatalyst Activation with a Lewis Base. *ACS Catal.* **2014,** *4*, 4377-4388. (h) vom Stein, T.; Meuresch, M.; Limper, D.; Schmitz, M.; Holscher, M.; Coetzee, J.; Cole-Hamilton, D. J.; Klankermayer, J.; Leitner, W. Highly Versatile Catalytic Hydrogenation of Carboxylic and Carbonic Acid Derivatives Using a Ru-Triphos Complex: Molecular Control over Selectivity and Substrate Scope. *J. Am. Chem. Soc.* **2014,** *136*, 13217-13225. (i) Chen, X.; Jing, Y.; Yang, X. Unexpected Direct Hydride Transfer Mechanism for the Hydrogenation of Ethyl Acetate to Ethanol Catalyzed by Sns Pincer Ruthenium Complexes. *Chem. Eur. J.* **2016,** *22*, 1950-1957. (j) Elangovan, S.; Garbe, M.; Jiao, H.; Spannenberg, A.; Junge, K.; Beller, M. Hydrogenation of Esters to Alcohols Catalyzed by Defined Manganese Pincer Complexes. *Angew. Chem. Int. Ed.* **2016,** *55*, 15364-15368. (k) Dub, P. A.; Scott, B. L.; Gordon, J. C. Why Does Alkylation of the N-H Functionality within M/NH Bifunctional Noyori-Type Catalysts Lead to Turnover? *J. Am. Chem. Soc.* **2017,** *139*, 1245-1260. (l) Yan, X.; Yang, X. Mechanistic Insights into the Iridium Catalysed Hydrogenation of Ethyl Acetate to Ethanol: A DFT Study. *Dalton Trans.* **2018,** *47*, 10172-10178.

(8) (a) Dub, P. A.; Henson, N. J.; Martin, R. L.; Gordon, J. C. Unravelling the Mechanism of the Asymmetric Hydrogenation of Acetophenone by [RuX_2(Diphosphine)(1,2-Diamine)] Catalysts. *J. Am. Chem. Soc.* **2014,** *136*, 3505-3521. (b) Dub, P. A.; Gordon, J. C. The Mechanism of Enantioselective Ketone Reduction with Noyori and Noyori-Ikariya Bifunctional Catalysts. *Dalton Trans.* **2016,** *45*, 6756-6781.

(9) Ito, M.; Ootsuka, T.; Watari, R.; Shiibashi, A.; Himizu, A.; Ikariya, T. Catalytic Hydrogenation of Carboxamides and Esters by Well-Defined Cp*Ru Complexes Bearing a Protic Amine Ligand. *J. Am. Chem. Soc.* **2011,** *133*, 4240-4242.

(10) Agapova, A.; Alberico, E.; Kammer, A.; Junge, H.; Beller, M. Catalytic Dehydrogenation of Formic Acid with Ruthenium-PNP-Pincer Complexes: Comparing N-Methylated and NH-Ligands. *ChemCatChem* **2019,** *11*, 1910-1914.

(11) Korstanje, T. J.; van der Vlugt, J. I.; Elsevier, C. J.; de Bruin, B. Hydrogenation of Carboxylic Acids with a Homogeneous Cobalt Catalyst. *Science* **2015,** *350*, 298-302.

(12) (a) del Pozo, C.; Iglesias, M.; Sánchez, F. l. Pincer-Type Pyridine-Based N-Heterocyclic Carbene Amine Ru(II) Complexes as Efficient Catalysts for Hydrogen Transfer Reactions. *Organometallics* **2011,** *30*, 2180-2188. (b) Fogler, E.; Balaraman, E.; Ben-David, Y.; Leitus, G.; Shimon, L. J. W.; Milstein, D. New CNN-Type Ruthenium Pincer NHC Complexes. Mild, Efficient Catalytic Hydrogenation of Esters. *Organometallics* **2011,** *30*, 3826-3833. (c) Sun, Y.; Koehler, C.; Tan, R.; Annibale, V. T.; Song, D. Ester Hydrogenation Catalyzed by Ru-CNN Pincer Complexes. *Chem. Commun.* **2011,** *47*, 8349-8351.

(13) Kim, D.; Le, L.; Drance, M. J.; Jensen, K. H.; Bogdanovski, K.; Cervarich, T. N.; Barnard, M. G.; Pudalov, N. J.; Knapp, S. M. M.; Chianese, A. R. Ester Hydrogenation Catalyzed by CNN-Pincer Complexes of Ruthenium. *Organometallics* **2016,** *35*, 982-989.

(14) Le, L.; Liu, J.; He, T.; Kim, D.; Lindley, E. J.; Cervarich, T. N.; Malek, J. C.; Pham, J.; Buck, M. R.; Chianese, A. R. Structure–Function Relationship in Ester Hydrogenation Catalyzed by Ruthenium CNN-Pincer Complexes. *Organometallics* **2018,** *37*, 3286-3297.

(15) Liang, Q.; Song, D. Reactivity of Fe and Ru Complexes of Picolyl-Substituted N-Heterocyclic Carbene Ligand: Diverse Coordination Modes and Small Molecule Binding. *Inorg. Chem.* **2017,** *56*, 11956-11970.

(16) Zeng, R.; Feller, M.; Diskin-Posner, Y.; Shimon, L. J. W.; Ben-David, Y.; Milstein, D. CO Oxidation by N_2O Homogeneously Catalyzed by Ruthenium Hydride Pincer Complexes Indicating a New Mechanism. *J. Am. Chem. Soc.* **2018,** *140*, 7061-7064.

(17) Groom, C. R.; Bruno, I. J.; Lightfoot, M. P.; Ward, S. C. The Cambridge Structural Database. *Acta Crystallogr. B* **2016,** *72*, 171-179.

(18) (a) Xu, Q.; Duan, W.-L.; Lei, Z.-Y.; Zhu, Z.-B.; Shi, M. A Novel Cis-Chelated Pd(II)–NHC Complex for Catalyzing Suzuki and Heck-Type Cross-Coupling Reactions. *Tetrahedron* **2005,** *61*, 11225-11229. (b) Liu, X.; Chen, W. Synthesis of Ruthenium(II) Complexes of Tetradentate Bis(N-Pyridylimidazolylidenyl)Methane and Their Reactivities Towards N- Donors. *Dalton Trans.* **2012,** *41*, 599-608. (c) Alabau, R. G.; Esteruelas, M. A.; Oliván, M.; Oñate, E.; Palacios, A. U.; Tsai, J.-Y.; Xia, C. Osmium(II) Complexes Containing a Dianionic Cccc-Donor Tetradentate Ligand. *Organometallics* **2016,** *35*, 3981-3995.

(19) Hauser, S. A.; Tonner, R.; Chaplin, A. B. Iridium Complexes of the Conformationally Rigid IBioxMe$_4$ Ligand: Hydride Complexes and Dehydrogenation of Cyclooctene. *Organometallics* **2015,** *34*, 4419-4427.

(20) Buhl, H.; Ganter, C. Tuning the Electronic Properties of an N-Heterocyclic Carbene by Charge and Mesomeric Effects. *Chem. Commun.* **2013,** *49*, 5417-9.

(21) Yang, X. H.; Yue, H. T.; Yu, N.; Li, Y. P.; Xie, J. H.; Zhou, Q. L. Iridium-Catalyzed Asymmetric Hydrogenation of Racemic Alpha-Substituted Lactones to Chiral Diols. *Chem. Sci.* **2017,** *8*, 1811-1814.

(22) Kuriyama, W.; Ino, Y.; Ogata, O.; Sayo, N.; Saito, T. A Homogeneous Catalyst for Reduction of Optically Active Esters to the Corresponding Chiral Alcohols without Loss of Optical Purities. *Adv. Synth. Catal.* **2010,** *352*, 92-96.

(23) Widegren, M. B.; Clarke, M. L. Manganese Catalyzed Hydrogenation of Enantiomerically Pure Esters. *Org. Lett.* **2018,** *20*, 2654-2658.

(24) (a) Teunissen, H. T.; Elsevier, C. J. Homogeneous Ruthenium Catalyzed Hydrogenation of Esters to Alcohols. *Chem. Commun.* **1998**, 1367-1368. (b) Coetzee, J.; Dodds, D. L.; Klankermayer, J.; Brosinski, S.; Leitner, W.; Slawin, A. M.; Cole-Hamilton, D. J. Homogeneous Catalytic Hydrogenation of Amides to Amines. *Chem. Eur. J.* **2013,**

19, 11039-11050. (c) Cui, X.; Li, Y.; Topf, C.; Junge, K.; Beller, M. Direct Ruthenium-Catalyzed Hydrogenation of Carboxylic Acids to Alcohols. *Angew. Chem. Int. Ed.* **2015,** *54*, 10596-10599. (d) Adam, R.; Bheeter, C. B.; Cabrero-Antonino, J. R.; Junge, K.; Jackstell, R.; Beller, M. Selective Hydrogenation of Nitriles to Primary Amines by Using a Cobalt Phosphine Catalyst. *ChemSusChem* **2017,** *10*, 842-846.

(25) Frisch, M. J.; Trucks, G. W.; Schlegel, H. B.; Scuseria, G. E.; Robb, M. A.; Cheeseman, J. R.; Scalmani, G.; Barone, V.; Petersson, G. A.; Nakatsuji, H.; Li, X.; Caricato, M.; Marenich, A. V.; Bloino, J.; Janesko, B. G.; Gomperts, R.; Mennucci, B.; Hratchian, H. P.; Ortiz, J. V.; Izmaylov, A. F.; Sonnenberg, J. L.; Williams; Ding, F.; Lipparini, F.; Egidi, F.; Goings, J.; Peng, B.; Petrone, A.; Henderson, T.; Ranasinghe, D.; Zakrzewski, V. G.; Gao, J.; Rega, N.; Zheng, G.; Liang, W.; Hada, M.; Ehara, M.; Toyota, K.; Fukuda, R.; Hasegawa, J.; Ishida, M.; Nakajima, T.; Honda, Y.; Kitao, O.; Nakai, H.; Vreven, T.; Throssell, K.; Montgomery Jr., J. A.; Peralta, J. E.; Ogliaro, F.; Bearpark, M. J.; Heyd, J. J.; Brothers, E. N.; Kudin, K. N.; Staroverov, V. N.; Keith, T. A.; Kobayashi, R.; Normand, J.; Raghavachari, K.; Rendell, A. P.; Burant, J. C.; Iyengar, S. S.; Tomasi, J.; Cossi, M.; Millam, J. M.; Klene, M.; Adamo, C.; Cammi, R.; Ochterski, J. W.; Martin, R. L.; Morokuma, K.; Farkas, O.; Foresman, J. B.; Fox, D. J. *Gaussian 16 Rev. B.01*, Wallingford, CT, 2016.

(26) (a) Lee, C.; Yang, W.; Parr, R. G. Development of the Colle-Salvetti Correlation-Energy Formula into a Functional of the Electron Density. *Phys. Rev. B* **1988,** *37*, 785-789. (b) Becke, A. D. Density-Functional Thermochemistry. III. The Role of Exact Exchange. *J. Chem. Phys.* **1993,** *98*, 5648-5652.

(27) Grimme, S.; Antony, J.; Ehrlich, S.; Krieg, H. A Consistent and Accurate Ab Initio Parametrization of Density Functional Dispersion Correction (DFT-D) for the 94 Elements H-Pu. *J Chem Phys* **2010,** *132*, 154104.

(28) Hay, P. J.; Wadt, W. R. Ab Initio Effective Core Potentials for Molecular Calculations. Potentials for K to Au Including the Outermost Core Orbitals. *J. Chem. Phys.* **1985,** *82*, 299-310.

(29) Ehlers, A.; Böhme, M.; Dapprich, S.; Gobbi, A.; Höllwarth, A.; Jonas, V.; Köhler, K.; Stegmann, R.; Veldkamp, A.; Frenking, G. A Set of F-Polarization Functions for Pseudo-Potential Basis Sets of the Transition Metals Sc-Cu, Y-Ag and La-Au. *Chem. Phys. Lett.* **1993,** *208*, 111-114.

(30) Roy, L. E.; Hay, P. J.; Martin, R. L. Revised Basis Sets for the Lanl Effective Core Potentials. *J. Chem. Theory Comput.* **2008,** *4*, 1029-1031.

(31) (a) Krishnan, R.; Binkley, J. S.; Seeger, R.; Pople, J. A. Self-Consistent Molecular Orbital Methods. XX. A Basis Set for Correlated Wave Functions. *J. Chem. Phys.* **1980,** *72*, 650-654. (b) McLean, A. D.; Chandler, G. S. Contracted Gaussian Basis Sets for Molecular Calculations. I. Second Row Atoms, Z=11–18. *J. Chem. Phys.* **1980,** *72*, 5639-5648.

(32) Marenich, A. V.; Cramer, C. J.; Truhlar, D. G. Universal Solvation Model Based on Solute Electron Density and on a Continuum Model of the Solvent Defined by the Bulk Dielectric Constant and Atomic Surface Tensions. *J. Phys. Chem. B* **2009,** *113*, 6378-6396.

(33) Cramer, C. J., In *Essentials of Computational Chemistry*, 2nd ed.; Wiley: Chichester, UK, 2004; 378-379.

(34) Macrae, C. F.; Edgington, P. R.; McCabe, P.; Pidcock, E.; Shields, G. P.; Taylor, R.; Towler, M.; van de Streek, J. Mercury: Visualization and Analysis of Crystal Structures. *J. Appl. Cryst.* **2006,** *39*, 453-457.

TABLE OF CONTENTS GRAPHIC

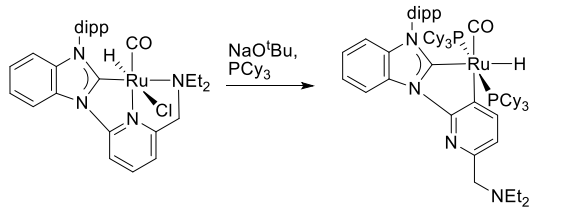

catalyzes ester hydrogenation ***with*** *added base*

catalyzes ester hydrogenation ***without*** *added base*